MICROSTRUCTURAL CHARACTERISATION AND CORROSION BEHAVIOUR OF TOP SURFACE OF TIG WELDED 2219−T87 ALUMINIUM ALLOY

G. Venkatasubramanian[a] , A. Sheik Mideen[a*], Abhay K Jha[b]
[a]Department of Chemistry, Sathyabama University, Jeppiaar Nagar, Chennai-600119, India
[b]Materials Characterization Division, Vikram Sarabhai Space Centre, Indian Space Research Organisation, Thiruvananthapuram–695022, India
smideen@yahoo.co.in

Abstract

The microstructural characterisation and corrosion behaviour of top surface of tungsten inert gas (TIG) welded 2219−T87 aluminium alloy (AA2219–T87) in 0.6 M NaCl solution was studied by optical microscopy, scanning electron microscopy (SEM), potentiodynamic polarisation, and electrochemical impedance spectroscopy (EIS). The optical microscopy and SEM analyses revealed that the welding of base metal (BM) with ER2319 filler alloy caused the formation of micro pores and micro cracks on the surface of weld zone (WZ) while the welding heat caused the dissolution and segregation of $CuAl_2$ intermetallic particles along the grain boundaries in the heat affected zone (HAZ). The anodic and cathodic branches of polarisation curves showed that the HAZ has lower corrosion resistance than WZ and BM. The decrease of charge transfer resistance of HAZ when compared to WZ and BM obtained by electrochemical impedance spectroscopy (EIS) further confirmed its higher corrosion rate in 0.6 M NaCl solution.

Keywords: AA2219-T87, EIS, SEM, Heat Affected Zone

1. Introduction

2219 aluminium alloy (AA2219) is a thermo-mechanically treatable Al-Cu alloy which on precipitation and aging follows the sequence: $\alpha \rightarrow \theta$ + GP zones $\rightarrow \alpha + \theta'' \rightarrow \alpha + \theta' \rightarrow \alpha + \theta$. The aluminium solid solution is indicated by α, the meta-stable phases are indicated by θ', θ″ and the stable precipitate by θ [1]. A proper heat treatment of AA2219 allows this alloy to be widely used for aircraft components [2-3]. The distribution of second phase intermetallic particles and effect of copper content on the corrosion behaviour of aluminium alloys was explained by many researchers [4-9]. AA2219-T87 is widely used for the fabrication of cryogenic propellant tanks due to its high strength and good weldabilitly [10-12].

During the fabrication process, the aluminium alloy plates and sheets are joined by friction stir welding (FSW), tungsten inert gas welding (TIG), electron beam welding (EB) etc. TIG welding process is commonly used to join AA2219 plates due to its inherent advantages of arc cleaning [13].Thermal cycles in welding process cause the chemical and micro structural changes. These changes affect the mechanical and corrosion properties of the welded joints. Mechanical properties like tensile strength, fracture and impact toughness are typically controlled by cross-sectional microstructure. But the corrosion and fatigue behaviour are influenced by top surface microstructure [14].

The corrosion resistance of cross sectional surface of AA2219 FSW in 3.5% NaCl solution at neutral pH has been reported and the results showed that the weld nugget was better than that of base metal [15]. Corrosion behaviour of AA2219 GTA and EB welds was compared in 3.5% NaCl in the cross sectional area and EB weld was reported as superior [16]. Corrosion behaviour of multipass friction stir processed (FSP) AA2219 alloy at different number of passes was investigated using potentiodynamic and EIS techniques in 3.5% NaCl at pH 10. Three pass and two pass FSP alloy showed better corrosion resistance in comparison to the single pass processed alloy. The same authors studied the above FSP AA2219 alloy using the same techniques at different rotations speed and reported that the corrosion resistance increased with increase in rotation speed [17,18]. Pitting corrosion behaviour of different weld nugget regions (top, middle and bottom) of FSW joints in AA2219-O was examined in 3.5% NaCl at neutral pH. It has been concluded that the base metal of AA2219-O is more susceptible to pitting corrosion and the order of corrosion resistance was top > middle > bottom > base material [19]. Electrochemical corrosion behaviour of different regions of TIG welded AA2219 was investigated in 3.5% NaCl at neutral pH using potentiodynamic polarization technique. The samples were prepared from transverse cross section by cutting at an angle of 45deg along the weld interface. The study concluded that partially melted zone (PMZ) was prone to more corrosion when compared to other regions [20]. Recently the corrosion behaviour of different regions of cross sectional area of AA2219−T87 welded plates in seawater was analysed and heat affected zone (HAZ) was prone to more corrosion than weld zone and base

metal in seawater [21]. Recently, Venkatasubramanian *et al* has compared and reported the corrosion behaviour of top and cross sectional phases of AA2219-T87 base metal in 3.5% NaCl solution [22].

Many investigations for corrosion behaviour of AA2219 are pertaining to the cross sectional area of joints. The present work reveals the corrosion behaviour of the top surface of different zones of gas tungsten arc welded AA2219-T87 plates in 0.6 M NaCl solution and compares the results with base metal (BM).

2. Experimental

Fig. 1 shows the schematic representation of tungsten inert gas (TIG) welded 2219−T87 aluminium alloy rolled plate used in the present investigation. The temper designation T8 represents solution heat treatment and cold working followed by artificial aging and 7 represents the percentage of cold work employed [23]. The plates were autogeneously alternating current TIG welded perpendicular rolling direction at a speed of 200 mm min^{-1}, under high purity Ar gas shielding. The ER 2319 alloy was used as filler wire and supplied at a feed rate of 2100 mm min^{-1} [24].

The chemical composition of parent metal and filler wire are given in Table 1. The working electrodes for corrosion studies were cut from the welded plates parallel to the rolling direction and perpendicular to welding direction in such a way the test specimens consisted of base metal (BM), weld zone (WZ) and heat affected zone (HAZ). The specimens were used in flat type with mirror smooth finish after mechanically abraded with different grades of silicon carbide sheets followed by 1 µm finish using rotating disc with non-aqueous diamond paste, degreased by acetone, washed with double distilled water and dried.

Except the zone under study, the rest of the zones were suitably masked with a red lacquer and further wrapped with Teflon tape. The Keller etchant [2.5ml HNO_3 (60%) + 1.5ml HCl (37%) + 1ml HF (48%) + 95 ml of double distilled water] was used to identify the HAZ and are located 3 mm away from weld zones on both sides. In all experiments 10mm×1mm was exposed in order to compare the results.

Potentiodynamic polarization tests were carried out according to ASTM standard G3–89 (ASTM G3-89, 2004)) using software based Bio-analytical system [BAS−Zahner, make IM6– electrochemical analyzer model using THALAS−Flink software]. The flat type working electrodes were categorized into BM, WZ and HAZ. A saturated calomel electrode coupled to a fine Luggin capillary as reference electrode and graphite electrode as counter electrode were used. The Luggin capillary was kept close to the working electrode to reduce the ohmic contribution. Freshly prepared 0.6 M NaCl was used as electrolyte. The polarization curves were determined by stepping the potential at a scan rate of 0.5mV/sec from –250 mV (SCE) to +250 mV vs SCE. All the experiments analyzed in this paper were performed at room temperature (25°C) and repeated for at least two times to get reproducibility.

The electrochemical impedance spectroscopy (EIS) measurements were carried out in 0.6 M NaCl using a potentiostat coupled to a frequency response analyzer system in the frequency range 100 k Hz. to 100 m Hz. with amplitude of 10 mV peak to peak using AC signals at open circuit potential. The working electrode consists of either BM or WZ or HAZ and graphite electrode and saturated calomel electrode were used as counter electrode and reference electrode respectively. Potentiodynamic polarization and EIS measurements were performed after initial delay of 10 minutes for the sample to reach a steady state condition.

The microstructure of the AA2219−T87 welded plates were characterized by using optical microscopy (Olympus GX 71 Inverted Metallurgical Microscope, Japan) and Scanning Electron Microscopy (SEM). Optical metallography was performed on samples with transverse cross section. The samples were mechanically abraded with different grades of silicon carbide sheets followed by 1µm finish using rotating disc with non-aqueous diamond paste followed by degreased with acetone and etching with Keller's etchant for about 30 to 60 seconds and used. SEM characterization was performed on samples using scanning electron microscope (HITACHI model) operating at 15kV.

3. Results and discussions

3.1 Potentiodynamic polarisation

Potentiodynamic polarisation curves of various zones of AA2219-T87 welded plate in 0.6M NaCl is shown in Fig.2. The various corrosion parameters obtained from Tafel plots are given in table 2. The open circuit potential for various zones of BM, WZ and HAZ are –0.712V, –0.680V and –0.630V respectively. These differences are due to the different chemical composition of base metal and filler metal. The corrosion potential (E_{corr}) of BM, WZ and HAZ have anodic shift from OCP. There is a considerable increase in corrosion current density (i_{corr}) for HAZ (1.2µA cm^{-2}). During welding the temperature in the HAZ varies from 490°C to 570°C. Due to this high temperature the dissolution and segregation of hardening precipitates, $CuAl_2$ takes place along the grain boundaries [16]. Further this causes redistribution and enrichment of copper in HAZ. The BM showed lower i_{corr} of 0.18µA cm^{-2} and it is due to higher anodic to cathodic area distribution [25]. The polarisation curves also reveal a higher cathodic slope for all regions. This is due to presence of main alloying element

copper and nobler $CuAl_2$ intermetallic particles (IMP). The i_{corr} observed for WZ is 0.43 μA cm^{-2} which is in between HAZ and BM.

3.2 EIS results

Nyquist curves of various zones of AA2219-T87 welded plate in 0.6M NaCl is shown in Fig.3. The various corrosion parameters obtained from Nyquist curves are given in table 2. The diameter of semicircle corresponding to charge transfer resistance (R_{ct}) indicates the corrosion rate. The BM showed maximum R_{ct} of 14 kΩ cm^2 when compared to WZ (9 kΩ cm^2) and HAZ (5.8 kΩ cm^2). This higher corrosion resistance of BM is due to the more homogeneous distribution of $CuAl_2$ IMPs in α-solid solution. The increase of the double layer capacitance (C_{dl}) for HAZ (1.5×10^{-2}μF cm^{-2}) further confirms the decreased corrosion resistance in 0.6 M NaCl. The relatively lower R_{ct} and increased capacitance showed the lower corrosion resistance of HAZ. This is essentially due to the acceleration of cathodic reaction. Presence of shrinkage pores; minute cracks and copper rich areas are responsible for lower R_{ct} in WZ when compared to BM. This is in well agreement with Tafel results obtained in the previous experiments.

3.3 Microstructural analysis

Optical micrograph of BM is shown in fig. 4a, in which finely divided black IMPs are homogeneously distributed along the grain boundaries within the matrix. The SEM images of BM in different magnifications are shown in fig. 5a,b. They reveal very clear distinct boundaries with whiter regions of IMPs distributed in the matrix. Presence of fine and homogeneously distributed IMPs is responsible for BM corrosion in 0.6 M NaCl solution. Fig 4c shows the optical micrograph of HAZ. Fig. 6a,b depicts the SEM images of HAZ in different magnifications. Segregation of more noble IMPs due to the higher temperature difference during welding along the grain boundaries is responsible for higher corrosion rate when compared to BM. Fig 4b shows the optical micrograph of WZ. Fig.7a,b depicts the of SEM images of WZ. The images show dendritic structure of copper rich areas in WZ which are randomly distributed due to welding heat. The presence of mild cracks which might have produced during polishing and shrinkage micro pores is the reason for relatively more corrosion rate of WZ than BM.

4. Conclusion

- The potentiodynamic polarisation and electrochemical impedance spectroscopy of different regions of top surfaces of TIG welded aluminium alloy 2219−T87 plate in 0.6 M NaCl solution follow the order of corrosion resistance: BM > WZ > HAZ.
- Presence of fine and homogeneously distributed IMPs is responsible for BM corrosion in 0.6 M NaCl solution.
- Segregation of more noble IMPs along the grain boundaries due to the high welding temperature is responsible for higher corrosion rate of HAZ when compared to BM.
- The presence of minute cracks which might have been produced during polishing; copper rich nobler areas and shrinkage micro pores is the reason for corrosion behaviour of WZ.

References

[1] Davis, J. R.,(1996): Aluminium and aluminium alloys, ASM Speciality Hand book, ASM International, Materials Park, OH, p.291.
[2] Source book on selection of and fabrication of aluminium alloys, ASM, Ohio, 1978.
[3] Standard practice for heat treatment of aluminium alloys, ASTM B 597-90, 1990.
[4] Robinson, M. J. (1982): Mathematical modeling of exfoliation corrosion in high strength aluminium Alloys, Corros. Sci., 22(8), pp.775-790
[5] Meletis, E. I.; Weiji Huang. (1991): The role of the T1 phase in the pre-exposure and hydrogen embrittlement of Al-Li-Cu alloys, Mater. Sci. and Engg. A, 148(2), pp.197- 209
[6] Keddam, M.; Kuntz, C.; Takenouti, H; Schustert, D; Zuili, D. (1997): Exfoliation corrosion of aluminium alloys examined by electrode impedance Electrochim. Acta, 42 (1), pp. 87-97
[7] Williams Stewart, W; Rajan Ambat; Debbie Price; Manthana Jariyaboon; Alison Davenport, J.; Andrew Wescott. (2003): Laser treatment method for improvement of the corrosion resistance of friction stir welds, Mater. Sci. Forum. 426, pp.2855-2860
[8] Birbilis, N.; and Buchheit, R. G. (2005): Electrochemical characteristics of intermetallic phases in aluminum alloys: An experimental survey and discussion, J. Electrochem. Soc., 152(4) pp.140-151
[9] Paglia, C. S; Buchheit, R. G. (2006): Microstructure, microchemistry and environmental cracking susceptibility of friction stir welded 2219-T87, Mater. Sci. and Engg. A, (429) pp.107-114.
[10] Speidel, M. O. (1975): Metall. Trans. A, (6A) pp.633-651
[11] J.R.Simmons, J. R.; Johnson, L.; Daech, A.; and Merschel. R.(1982): Mater. Perf., June, pp14-18.
[12] Crane, C. H.; and Smith, W. G. (1961): Weld. Res. Suppl., Jan. pp33-40
[13] Ghosh, B. R.; Gupta, R. K.; Biju, S.; Sinha, P. P.(2007): Modified welding technique of a hypo-eutectic Al-Cu alloy for higher mechanical properties, J. Solid Mechs. and Mater. Engg., (4)1, pp.469-479
[14] Ishchenki, A; A.V.Lozovskaya, A. V. Ya.; and Sayenko, I. M. I.(1989): Weld Intl., (8) pp.654-656
[15] Balasrinivasan, P; Arora, K.S.; Dietzel. W.; Pandey, S.; Schaper, M. K.(2010): Characterization of microstructure, mechanical properties and corrosion behavior of an AA2219 friction stir weldment, J Alloys Compd. 492 (1-2) pp.631-637.
[16] Koteswara Rao, S. R.; Madhusudhan Reddy. G; Srinivasa Rao, K.; Kamaraj, M.; Prasad Rao, K(2005): Reasons for superior mechanical and corrosion properties of 2219 aluminum alloy electron beam welds, Mater. Charac., 55(4-5) pp.345- 354.
[17] Surekha, K.; Murthy, B. S.; and Prasad Rao, K. (2008): Microstructural characterization and corrosion behavior of multi pass friction stir processed AA2219 aluminium alloy, Suface & Coatings Technology, 202 pp. 5057-4068.

[18] Surekha, K; Murthy, B. S.; and Prasad Rao, K.(2009): Effect of processing parameters on the corrosion behavior of fricitn stri processed AA2219 aluminium alloy, Solid state sciences, (11) pp.907-917
[19] Weifeng, Xu: Jinhe Liu.(2009): Microstructure and pitting corrosion of friction stir welded joints in 2219-O aluminium alloy thick plate, Corrosion science, 51 pp.2743-2751
[20] Venugopal, A; Sreekumar, K; Raja, V. S. (2010): Effect of repair welding on electrochemical corrosion and stress corrosion cracking behavior of TIG welded AA2219 aluminium alloy in 3.5% NaCl Solution, Metall Mater Trans A, 41(12) pp.3151-3160.
[21] Venkatasubramanian, G; Sheik Mideen, A; Abhay K Jha. (2012): Corrosion Behavior of Aluminium Alloy Aa2219−T87 Welded Plates in Sea Water, Indian Journal of Science and Technology, (5) 11, pp3578-3583
[22] Venkatasubramanian, G; Sheik Mideen, A; Abhay K Jha. (16 – 18 September 2010): Comparative study of electrochemical characteristics of different phases of aluminium alloy AA2219-T87 plate in 3.5% NaCl and seawater, 15th National Congress on Corrosion Control, .
[23] In 'Aluminium standards and data', (1982)159, Washington DC, USA. The Aluminium Association
[24] Venkata Narayana, G.; Sharma, V. M. J.; Diwahar, V; Sreekumar. K; Prasad, R. C.(2004): Fracture behaviour of aluminium alloy 2219– T87 welded plates, Sci. and Tech. of Weld. and Joining, 9(2) pp.121-130
[25] Holingsworth, E. H.; and Hunsicker, H. Y.(2001): Corrosion of aluminium and aluminium alloys, ASM Hand Book, Vl.(13) pp.583-609.

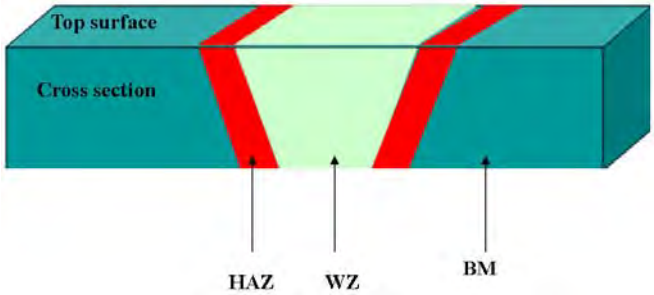

Fig.1. Locations of test specimens of Base metal (BM), heat affected zones (HAZ),weld zone (WZ)

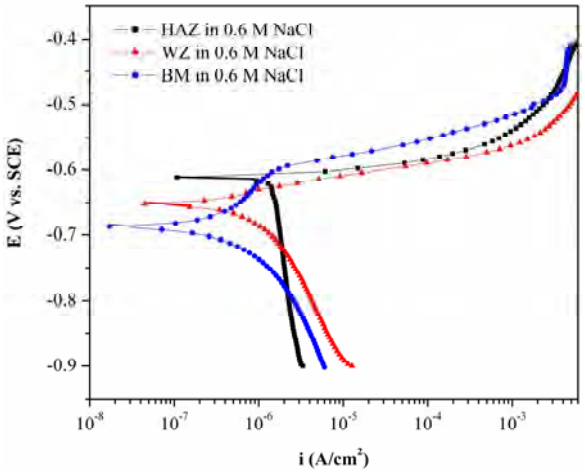

Fig.2. Potentiodynamic polarization curves for top surface AA2219-T87 welded plate in 0.6 M NaCl

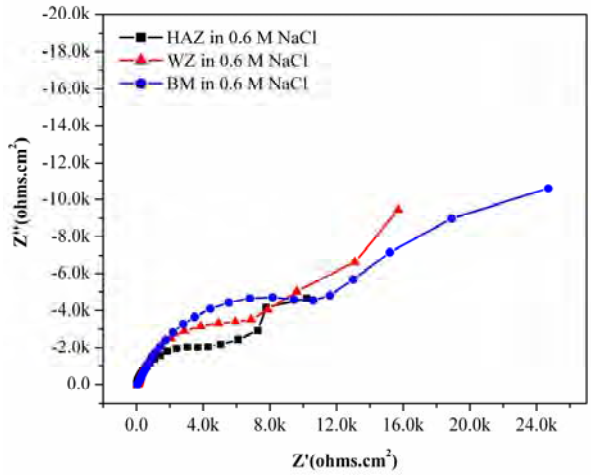

Fig.3 Nyquist plot for top surface of AA2219-T87 welded plate in 0.6 M NaCl

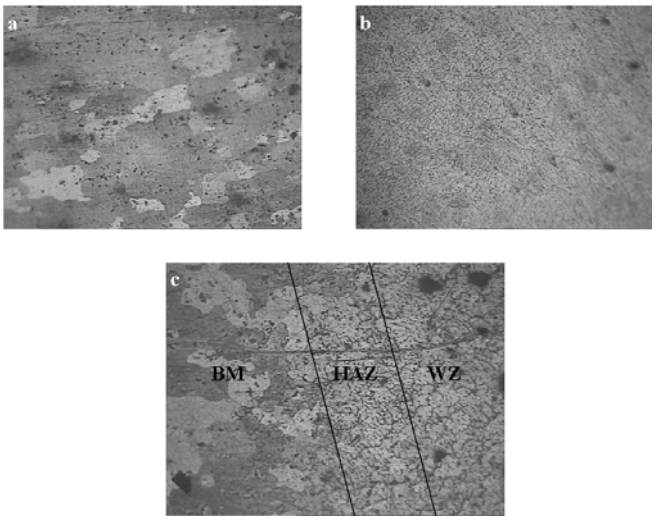

Fig.4 100X Microstructure of (a) BM, (b) WZ, (c) HAZ

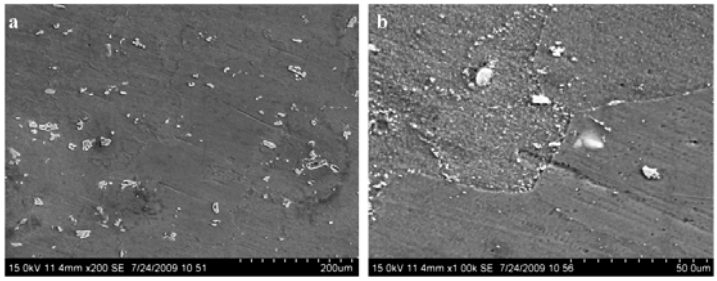

Fig. 5 SEM image of BM (a) Lower magnification (b) Higher magnification

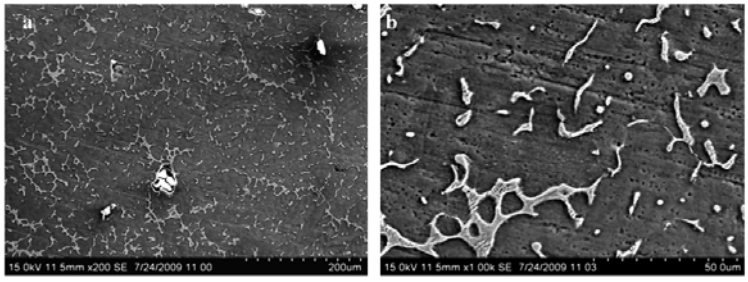

Fig. 6 SEM image of HAZ (a) Lower magnification (b) Higher magnification

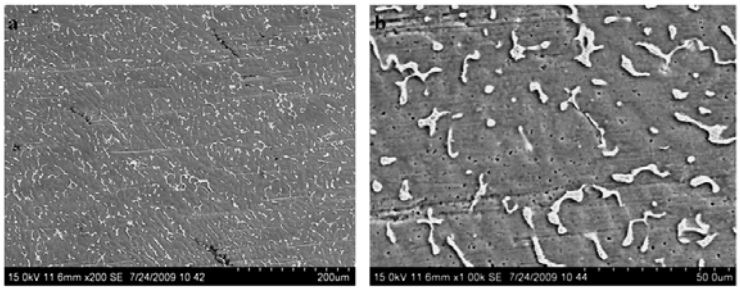

Fig.7 SEM image of WZ (a) Lower magnification (b) Higher magnification

Table 1 Nominal composition of AA2219-T87 and ER2319 filler metal (% by mass).

Alloy	Elements %							
	Cu	Mn	Zr	V	Ti	Fe	Si	Al
AA2219	5.95	0.27	0.12	0.09	0.06	0.12	0.05	Balance
ER2319	6.10	0.29	0.15	0.1	0.15	0.10	0.04	Balance

Table 2 Corrosion parameters obtained from Tafel plots and Nyquist curves for different zones of top surface of AA2219-T87 welded plates in 0.6 M NaCl

Various Zones	OCP (V vs SCE)	i_{corr} ($\mu A\ cm^{-2}$)	E_{corr} (V vs SCE)	R_{ct} ($k\Omega\ cm^2$)	C_{dl} ($\mu F\ cm^{-2}$)
BM	-0.712	0.18	-0.689	14	$6.2x10^{-3}$
WZ	-0.680	0.43	-0.642	9	$1.1x10^{-2}$
HAZ	-0.630	1.2	-0.614	5.8	$1.5x10^{-2}$